BWatch: A Non-invasive Blood Leakage Detection Device using Robust Reflectance-based Sensing*

Chee How Tan[1], Jien-Yi Khaw[1], Ying Ching Wong[2], Chang Yin Chionh[3] and Shaohui Foong[1]

***Abstract*— The insertion and removal of central venous catheter are associated with potentially fatal bleeding risk. This paper presents the design and development of BWatch, an effective stand-alone electronic device that continuously monitors the catheter insertion and extraction site for critical re-bleeding, that alerts medical staff immediately for proper care. The device employs novel non-invasive methods for blood detection. A capacitive circuit was designed to detect the presence of the moisture on the bandage. Exploiting the unique light absorption spectra of haemoglobin, the device subsequently illuminates and measures the absorbance of green light for accurate detection. Principal Component Analysis (PCA) was used to derive a suitable green LED light intensity and a single-value threshold from a triple-channel RGB light sensor for robust detection across medium. Finally, an experimental bench test was conducted in Changi General Hospital (CGH) and BWatch achieved 100% detection accuracy across 10 experimental run with real blood samples.**

I. INTRODUCTION

Central venous catheters (CVCs) are commonly adopted in clinical practice to administer medications, fluids, nutrition, and for medical procedures such as haemodialysis. However, the insertion and removal of CVCs are associated with potentially fatal haemorrhage risk (i.e. bleeding) and other complications [1][2]. After insertion or extraction, the wound site requires active medical supervision by medical staff for critical re-bleeding at 15 mins and 30 mins interval for the first and next two hours window respectively [3]. In this work, a smart medical device to afford continuous real-time monitoring of the wound site, alerting medical personnel immediately of bleeding episodes for proper care, is presented.

The extensive research conducted on optical sensing techniques for non-invasive reflectance pulse oximetry and glucose monitoring are highly relevant to this work. The optical characteristics of the object at one or more wavelength are exploited. In the case of pulse oximetry, the light absorption difference between oxygenated haemoglobin (HbO_2) and deoxygenated haemoglobin (Hb) in blood at multiple spectral regions, such as green, red and infrared (IR) region are used to estimate oxygen saturation level [4][5][6][7].

*This work is supported by the National Health Innovation Centre (NHIC) Innovation to Develop (I2D) Grant (NHIC-I2D-1608124) and the SUTD-MIT International Design Centre (IDC).

[1]The authors are with the Engineering Product Development Pillar, Singapore University of Technology and Design (SUTD), 8 Somapah Road, Singapore 487372. foongshaohui@sutd.edu.sg

[2]The author is with the Department of Electronic Engineering, City University of Hong Kong, Kowloon, Hong Kong.

[3]The author is with the Division of Renal Medicine, Changi General Hospital, 2 Simei Street 3, Singapore 529889.

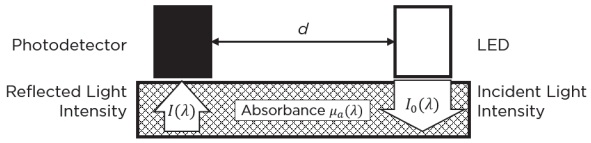

Fig. 1. A simplified schematic illustrating the model variables used.

Similarly, non-invasive glucose monitoring device leverages on the scattering property of glucose molecules under IR light for glucose concentration estimation in blood [8][9]. Hence, reflectance-based sensing approach have been proven to be a reliable non-invasive monitoring technique, and this work proposes utilising the same principle for haemoglobin detection in fluid.

BWard, an early design prototype for post-catheter extraction haemorrhage detection, has been presented in [3]. It relies on measuring the absorbance of a sample at two different wavelengths for reliable haemoglobin detection. Firstly, an IR emitter-photodiode pair, with dominant wavelength $\lambda_D = 950$ nm, detects fluid presence. Secondly, a green light emitter-detector pair ($\lambda_D = 528$ nm) subsequently determines if the fluid contains haemoglobin, which is an indicator of blood presence. Lastly, an additional contact resistive-based sensor module measures the electrical resistivity of the gauze for reliable detection of fluid presence. Consequently, BWard's operation requires direct contact with blood-soaked bandage. For sterility reason, direct contact is undesirable.

In this paper, a new simplified and non-invasive design (BWatch, see Fig. 5) is proposed. BWatch emits only a single wavelength for reliable detection of blood presence in the bandage. For moisture detection, a capacitive-based sensor that does not require direct contact with blood-soaked bandage is presented.

II. METHODS

This section presents the theoretical background of modelling light intensity attenuation for blood identification, followed by the use of principal component analysis (PCA) for finding a feature vector for dimensionality reduction, and lastly using a binary support-vector machine (SVM) for accurate haemoglobin presence classification and detection.

A. Reflectance-based Blood Detection using Green Light

Similar to reflectance pulse oximetry approach [5][7], the reflected light intensity from a wet bandage, $I(\lambda)$, can be described using Beer-Lambert's law,

$$I(\lambda) = I_0(\lambda) \exp(-\mu_a(\lambda) \cdot d) \quad (1)$$

978-1-7281-3458-1/19/$31.00

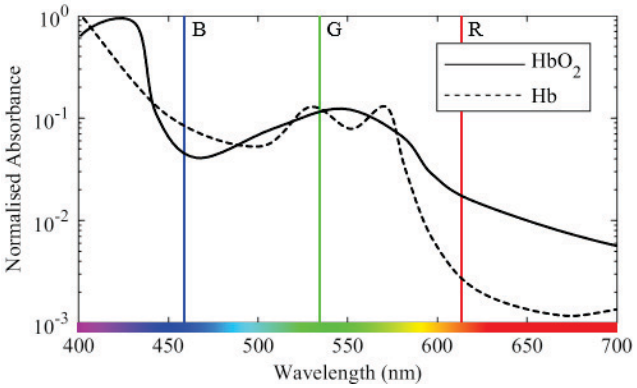

Fig. 2. The normalised absorption spectrum of HbO_2 and Hb [7] are illustrated. The red, blue, and green vertical lines represents the peak sensitivity of the respective channels of the TCS34725 RGBC sensor [11].

where λ is incident light source wavelength, $I_0(\lambda)$ is the incident light source intensity, $\mu_a(\lambda)$ is the absorption coefficient of the fluid medium, and d is the distance between the light emitter and detector. The model variables are illustrated in Fig. 1.

In the case of blood-soaked bandage, the $\mu_a(\lambda)$ can also be expressed as the sum of the molar extinction coefficient $\epsilon(\lambda)$ multiplied by the concentration C of HbO_2 and Hb

$$\mu_a(\lambda) = \epsilon_{\text{HbO}_2}(\lambda) \cdot C_{\text{HbO}_2} + \epsilon_{\text{Hb}}(\lambda) \cdot C_{\text{Hb}} \quad (2)$$

$$= \epsilon_{\text{blood}}(\lambda) \cdot C_{\text{blood}} \quad (3)$$

where $\epsilon_{\text{blood}} = \frac{1}{2}(\epsilon_{\text{HbO}_2} + \epsilon_{\text{Hb}})$ and C_{blood}, C_{HbO_2} and C_{Hb} is the concentration of blood, HbO_2 and Hb respectively.

For the purpose of haemoglobin detection, it is assumed that $C_{\text{blood}} = C_{\text{HbO}_2} = C_{\text{Hb}}$, making possible the simplification of (2) to (3). Hence, a non-zero C_{blood} results in attenuation of the reflected light intensity measured, $I(\lambda)$, which is indicative of blood presence.

Using (3), (1) can then be rewritten as

$$I(\lambda) = I_0(\lambda) \exp\left(-\epsilon_{\text{blood}}(\lambda) \cdot C_{\text{blood}} \cdot d\right) \quad (4)$$

The absorbance spectrum of HbO_2 and Hb in the visible light spectrum [7] is illustrated in Fig. 2, overlayed with the dominant wavelength of commercially accessible low-cost light-emitting diode (LED) [10] and color sensor [11]. Evidently, green light with dominant wavelength $\lambda_D = 525$nm is ideal for haemoglobin detection as it has the highest absorbance relative to red and blue light. This work assumes that the absorbance of haemoglobin in the green spectral region is appreciably higher than other similarly coloured haemoglobin-absent red fluid, making possible the distinction between blood and the latter. This assumption will be empirically proven in the Section III (Results) later.

However, the reflected light intensity measured are often mixed with unwanted ambient light. Ambient light leaks into the photo-detector because of variability in tightness when medical staff secures the device to the bandage, the irregular surface of the bandage, and etc. To reduce the measurement variability, a color sensor which outputs clear channel measurement indicative of the ambient lighting is desired. Assuming that ambient light have equal proportion of RGB components, the normalised light intensity $\hat{I}(\lambda)$ is less susceptible to changes in environment lighting, thus the degree of ambient light leakage. Then, (4) becomes

$$\hat{I}(\lambda) = \hat{I}_0(\lambda) \exp\left(-\epsilon_{blood}(\lambda) \cdot C_{blood} \cdot d\right) \quad (5)$$

where $\hat{I}(\lambda) = I(\lambda)/I_C$, $\hat{I}_0(\lambda) = I_0(\lambda)/I_C$, and I_C is the clear light intensity measured.

B. Feature Extraction and Dimensionality Reduction using Principal Component Analysis

For haemoglobin detection, a straightforward and naive method would be to base the decision solely on the proportion of green light $\hat{I}(\lambda = 525\text{nm})$ measured. For robust detection, however, this work proposes using the reflected light intensity measurements at the red, green, and blue (RGB) spectral region using a single color sensor. Principal component analysis (PCA) is introduced to extract representative features in the dataset instead. PCA assumes the correlation in the RGB measurements and exploits it to extract unique features, known as principal components, that maximises the variance in the new feature space [12].

The assumption of inherent correlation in the measured RGB intensity is valid due to two factors. Firstly, low-cost RGB sensors has appreciable cross-talk between the different color channels [11]. For example, an input irradiance by of a narrow-band green light with dominant wavelength $\lambda_D = 525$ nm with spectral halfwidth of 35 nm results in a typical 14.5%, 72.5% and 27.5% output in the red, blue and green channel of the color sensor respectively [11]. Secondly, the normalisation step introduced to reduce the effect of ambient light leakage results in dependency between the normalised RGB light measurement. For example, an increase in proportion of one color component (e.g. red light) correlates to a reduction in proportion of the remaining components (e.g. blue and green). These inherent correlations are exploited to find principal components which are linear combination of the original input data.

The k^{th} principal component (PC) z_k is given by

$$\boldsymbol{z}_k = \boldsymbol{\alpha_k}\hat{\boldsymbol{I}} = \alpha_{k1}\hat{\boldsymbol{I}}(\boldsymbol{R}) + \alpha_{k2}\hat{\boldsymbol{I}}(\boldsymbol{G}) + \alpha_{k3}\hat{\boldsymbol{I}}(\boldsymbol{B}) \quad (6)$$

where $\hat{\boldsymbol{I}}(\boldsymbol{R}), \hat{\boldsymbol{I}}(\boldsymbol{G}), \hat{\boldsymbol{I}}(\boldsymbol{B})$ are the normalised RGB light intensity measured and $\boldsymbol{\alpha_k}$ is the feature vector of the k^{th} PC, which have unit length (i.e. $||\boldsymbol{\alpha_k}||_2 = 1$).

The k^{th} PC is derived from the singular-value decomposition or the eigenvectors of the covariance matrix Σ where

$$\boldsymbol{\Sigma} = \hat{\boldsymbol{I}}\hat{\boldsymbol{I}}^T/n \quad (7)$$

The k^{th} column of $\boldsymbol{P} = [\boldsymbol{\alpha_1}, \boldsymbol{\alpha_2}, \boldsymbol{\alpha_3}]$, $\boldsymbol{\alpha_k}$ contains the coefficients of the k^{th} PC, and corresponding eigenvalue indicates the relative order of the PCs. Significantly, the eigenvector with the highest associated eigenvalue is the 1^{st} PC.

The variance of the k^{th} PC is defined as

$$\sigma_{zk} = \frac{1}{N-1}\sum_{i=1}^{N} |z_{k,i} - \bar{z}_k|^2 \quad (8)$$

where N is the sample size, and $\bar{z}_k$ is the sample mean. The variance of the original RGB components prior to the PCA transform are denoted as σ_R, σ_G, and σ_B respectively.

C. Blood Classification and Detection

For real-time detection, a simple threshold-based method is proposed. The threshold is determined by computing the decision boundary using binary SVM with linear kernel, trained offline using m labelled training examples consisting of blood and non-blood fluid medium. Assuming linearly separable data, the SVM minimises the objective function [13]

$$\min_{\beta,b} \frac{1}{2}||\beta||_2 - \sum_j \alpha_j(y_j(x_j'\beta + b) - 1) \tag{9}$$

where x_j is the j-th data point, and y_j is the label $\{+1, -1\}$ of the x_j corresponding to blood and non-blood respectively, β is the normal vector to the separating hyperplane, b is the bias, and α_j is a positive nonzero Langranger multiplier enforcing the classification constraint.

The margin γ, defined by $2/||\hat{\beta}||$, defines the maximal distance normal to the hyperplane with no interior data points. A larger margin is indicative of better class separability.

III. Results

This section presents the hardware implementation of the proposed prototype, BWatch, followed by the detail of the various experimental investigations.

A. Proposed Prototype: BWatch

BWatch (see Fig. 5) has a compact circular form factor, measuring 48mm diameter and weighs 19.25g. The key components of BWatch are an indium gallium nitride (InGaN) LED with dominant wavelength $\lambda_D = 525$nm to provide illumination, and a TCS3472 color sensor that measures reflected red, green, blue (RGB) light intensity. A capacitive sensor senses moisture on the bandage and activates the green LED for blood detection. Fig. 3(a) - (c) illustrates the mode of operation of BWatch when blood presence is detected in the bandage, and Fig. 3(d) when no blood presence is detected. A low-power ATSAMD21G microprocessor runs a lightweight algorithm, and controls the buzzer to sound when blood presence is detected. A 2MB on-board FLASH storage stores critical data for debugging and troubleshooting. The on-board electronics are powered by a replaceable and rechargable LIR2032 40mAh battery.

The electrical schematics of the key circuitry of BWatch are shown in Fig. 6. The capacitive moisture sensor is a copper pad (labelled as T1) which acts as the cathode pad. A capacitor, given a range from 0μF to 0.05μF, connected to T1 is used to vary the sensitivity of the moisture sensor. The TCS34725 RGB light sensor communicates to the Atmel ATSAMD21G MCU, (Microcontroller Unit) using I^{2}C protocol. The green LED is directly connected to the MCU, and switches on which an active-high input sent from the MCU. The buzzer is connected to the LIR2032 battery. The buzzer is connected in series to a MOSFET, and a pulse-width-modulated (PWM) signal sent from the MCU controls the activation of the buzzer. A diode is used to prevent any backflow current since the buzzer has an input voltage range of 3V to 5V.

B. Experimental Setup

A custom-made experimental rig was designed and developed to simulate bleeding at site of catheter insertion/extraction. The rig consist of the plastic enclosure with flat surface on the top to emulate the large surface of a human skin. The wound site is simulated by a hole, which is punctured at the centre of the box, and a plastic tube is connected from below to transport the fluid sample to the site. A peristaltic pump transfers the test fluid from a beaker to the bleeding site. The speed and direction of the fluid flow is controlled by a pump controller operating in three mode: namely forward, reverse, and pause mode.

To closely emulate the clinical scenario, the most common bandaging method was applied at the wound site. Firstly, two ply of gauze swab (Smith & Nephew) were placed over the wound site. Secondly, a layer of film dressing (3M Tegaderm) was applied to secure the gauze to the skin. Lastly, BWatch was placed in a plastic ziploc bag and secured to the bandage and the patient using surgical tape. Significantly, BWatch does not have direct contact to the gauze swab, as compared to BWard [3].

A total of six different medium were chosen to collect training examples to 1) determine the optimal green light intensity and 2) derive the decision boundary of the binary SVM classifier. The medium chosen were clean dry gauze, and gauze soaked in tap water, saline (0.9% sodium chloride), unsweetened pure pomegranate juice, red food-grade dye, and real blood. Tap water and saline were selected to emulate a soaked gauze due to accidental spillage of drinking water and natural perspiration respectively. Pomegranate and red dye are red fluid chosen to evaluate the robustness of the device to distinguish blood from other similarly coloured solution.

C. Effects of Light Intensity

The first experiment investigates the effects of light intensity on σ_{z1}, the 1st PC variance 1$^{\text{st}}$ PC, and σ_R, σ_G, and σ_B, which are the variance of normalised RGB data respectively. The results are shown in Fig. 7. Recall the variance of 1$^{\text{st}}$ PC and the normalised RGB proportion data are calculated using (8). A larger variance is desirable as it is beneficial to the subsequent classification step. The light intensity of the green LED was controlled by varying the duty cycle of the input pulse-width-modulated (PWM) signal. The percentage duty cycle of $[0, 100]$ output by the microcontroller corresponds to the 8-bit input $\boldsymbol{u}$ of $[0, 255]$. At each intensity level, u_i, 4 samples from the RGB sensor $\boldsymbol{x}_i$ were recorded. The experiment was repeated three times for consistency, across all six mediums. Hence, a total of 12 samples per intensity per medium are collected.

Fig. 7 shows the results the normalised variance of the 1^{st} PC, and RGB component against the intensity level tested. The normalised variance was obtained by dividing the sample

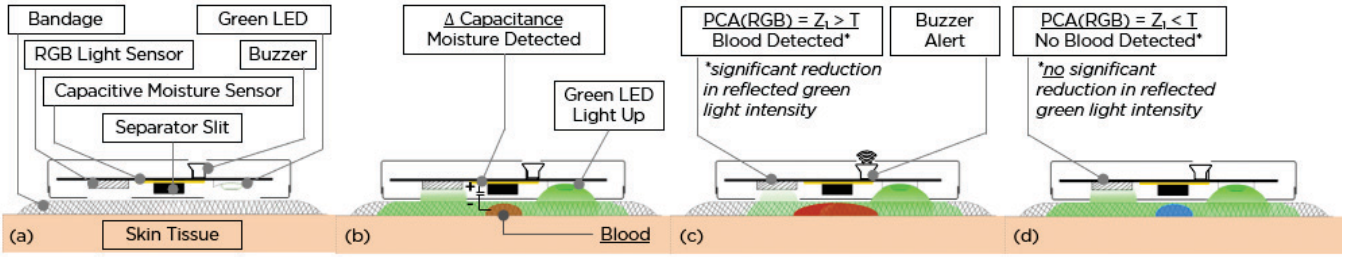

Fig. 3. The simplified overview of BWatch operation is illustrated. The key components are indicated in (a). Firstly, moisture presence in the gauze results in a change in capacitance of the moisture sensor, triggering the green LED to light up (b). Secondly, the light sensor measures the reflected RGB light intensity to determine blood presence (c). Lastly, if the measurement passed a threshold T, the buzzer sounds to alert nearby medical staff (c). If the required threshold is not passed, the device continues to monitor (d).

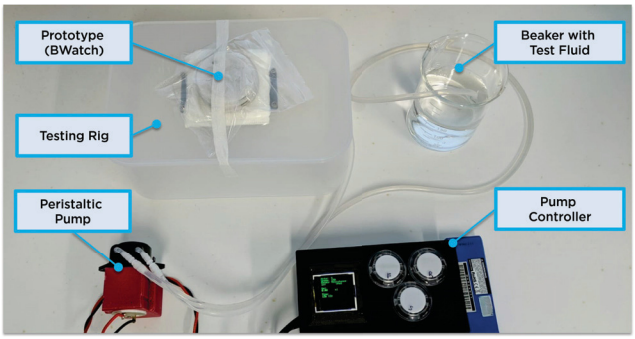

Fig. 4. The key components used in the experimental setup are illustrated. BWatch was wrapped in a plastic ziploc bag and placed aboved the film dressing that secures the gauze swab to the box.

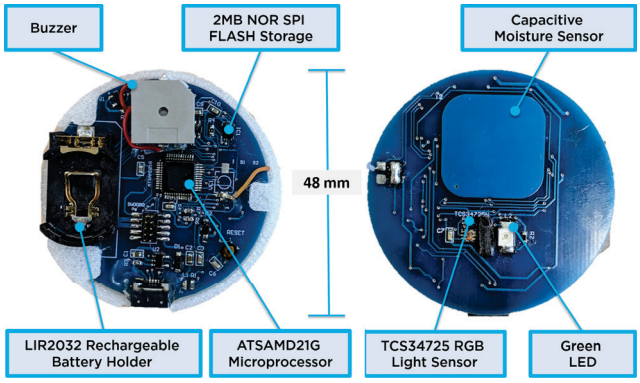

Fig. 5. The key components of BWatch are illustrated. The green LED is used to illuminate the bandage, and the TCS34725 RGB light sensor measures the reflected light intensity.

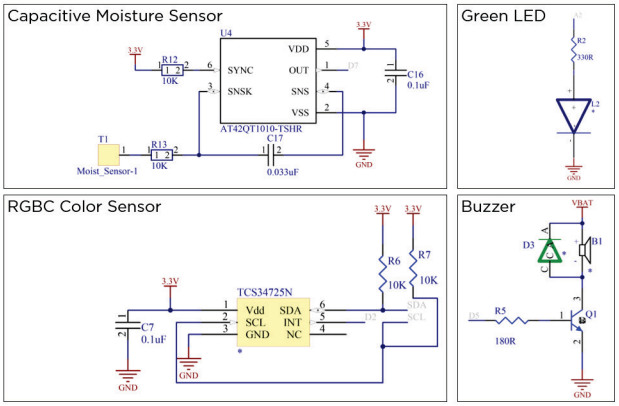

Fig. 6. The electrical schematics for the capacitive moisture sensor, light emitter and color sensor, and buzzer are shown.

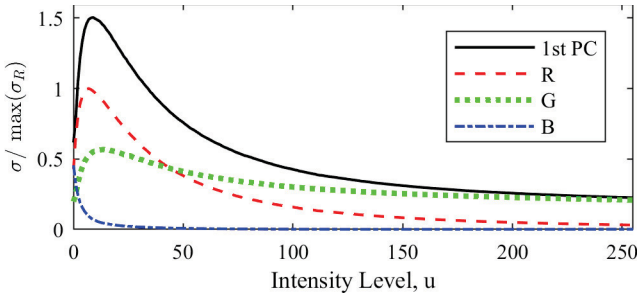

Fig. 7. The effects of the incident light intensity on the variance of the 1st Principal Component (1st PC). The maximum variance occur at intensity level $u^* = 9$.

variance by the $\max(\boldsymbol{\sigma}_R)$. It is observed that the variance increases with the increased light intensity level initially. The maximum variance for the 1st PC, red and green data are observed at $u = 9$. Further increment of the light intensity results in an exponentially drop in the resulting variance. The optimal intensity $u^* = 9$ was selected for subsequent experimentations.

The variation of the 1st PC was compared to red, blue, and green measurements recorded at the optimal intensity input $u^* = 9$ as shown in Fig 8. Intendedly, the 1st PC displayed the highest variance between blood and the other non-blood medium, followed by red, green, and blue components respectively. The variance are summarised in Table II. Significantly, the 1st PC resulted in a 50% increase in variance compared to red (the next highest variance).

D. Optimal PCA and Detection Performance

At the optimal intensity, $u^* = 9$, the coefficients of the $\hat{I}_R$, $\hat{I}_G$, $\hat{I}_B$ are listed in Table I. Evidently, the 1^{st} PC points in the direction of $\hat{I}_R$ and $\hat{I}_G$, with a greater weightage given to the former. The scatter plot of $\hat{I}_R$ against $\hat{I}_G$ are shown in Fig. 11. Significantly, the high absorbance characteristic of blood in the green spectrum results in a lower proportion of green light reflected. In addition, the blood reflects an appreciably higher proportion of red light compared to non-

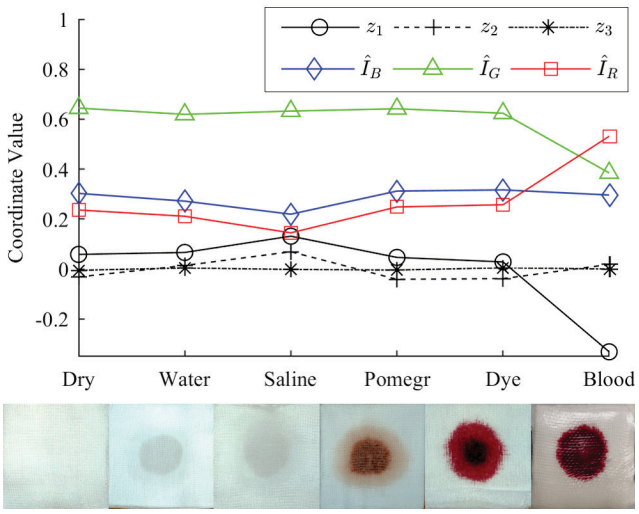

Fig. 8. The values of three principal components, and the normalised red, blue and green intensity measured are visualised across the different medium tested. The physical appearance of the gauze in the different medium are shown.

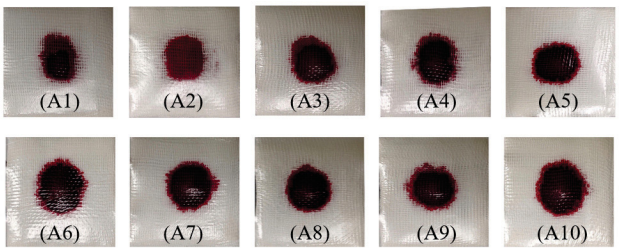

Fig. 9. The size of the blood stain on the gauze swab across the 10 clinical experiments with $C_{\text{blood}} = 100\%$. The mean blood blob size is 1000mm^2 and the min and max size is 874mm^2 and 1165mm^2 respectively.

blood medium, which includes pomegranate and red dye.

The 12 data samples collected from each medium in the previous experiment at $u^* = 9$ and the computed 1st PC was used for offline training of a binary SVM with linear kernel. The decision boundary and the training examples of blood and non-blood medium (i.e. dry, water, saline, pomegranate and red dye) are shown in Fig. 10. The boundary for blood detection is at $z_1 = -0.19$, with a margin of 0.56. Compared to a heuristically-driven approach of illuminating the gauze at maximum intensity $u = 255$ results in a sub-optimal variance as shown in Fig. 7. At $u = 255$, the 1st PC is almost equivalent to relying solely on the green channel measurements. The threshold for blood detection is at $z_1 = -0.06$ and a margin of 0.10

The classification algorithm based on the 1^{st} was validated with across 10 clinical experiments with real blood. Across all experiments, BWatch achieved 100% detection rate. The validation data are shown together with the training examples in Fig. 10.

The detection time and the area of the blood blob are recorded in Table IV. The detection time was computed using $t_{\text{d}} = t_{\text{alert}} - t_{\text{start}}$, where t_{alert} is the time the buzzer sounds and

TABLE I

FIRST THREE PCS AT OPTIMAL AND SUB-OPTIMAL INTENSITY

Component Number, k	1	2	3
Coefficient	Optimal (u = 9)		
Red, α_{k1}	0.80	-0.31	-0.51
Green, α_{k2}	0.59	-0.52	-0.61
Blue α_{k1}	-0.08	-0.79	0.60
Cumulative Variation	93.77	99.88	100.00
Coefficient	Sub-Optimal (u = 255)		
Red α_{k1}	-0.28	-0.94	0.21
Green α_{k2}	0.96	-0.28	0.06
Blue α_{k3}	0.00	0.22	0.96
Cumulative Variation	93.40	99.81	100.00

TABLE II

COMPARISON OF VARIABLE VARIANCE BEFORE AND AFTER PCA

Variable	1st PC σ_{k1}	Red σ_R	Blue σ_G	Green σ_B
Variance	0.023	0.015	0.0086	0.011

t_{start} is the time the peristaltic pump is started. The blood blob size was determine using the Image Processing Toolbox in MATLAB. The cropped RGB images of the gauze (see Fig. 9) are first converted into HSV images. A HSV threshold was applied to extract the size of blood blob (in pixel) from the resulting image. The blob area A_{blob} was calculated using $A_{\text{blob}} = A_{\text{gauze}} \cdot \frac{N_{\text{blob}}}{N_{\text{image}}}$ where A_{gauze} is the known area of the 75mm by 75mm gauze, N_{blob} is the size of the blood blob (in pixel) and N_{image} is the image pixel size. The mean size of the blood blob is 1000mm^2 with a standard deviation of 96mm^2, and the detection time averages at 4.88s with a standard deviation of 0.85s.

E. Performance Evaluation with Previous Work

The proposed method for blood detection using PCA is compared with the approach presented in [3]. In [3], the authors proposed using only the reflected green light intensity directly, and applying a simple thresholding method to determine blood presence. The results using the experimental data obtained in this work is shown Fig. 12. Generally, the

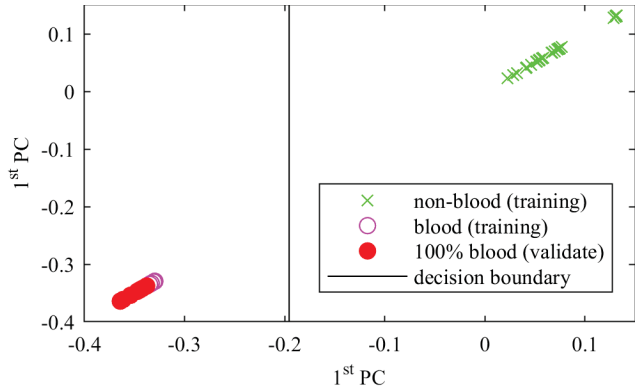

Fig. 10. The scatter plot of the 1^{st} PC of the training and validation dataset are illustrated.

TABLE III
SVM MARGIN AT OPTIMAL AND SUB-OPTIMAL INTENSITY

Intensity	Optimal $u = 9$		Sub-Optimal $u = 255$	
Method	PCA	RGB	PCA	RGB
Margin γ	0.56	0.36	0.10	0.10

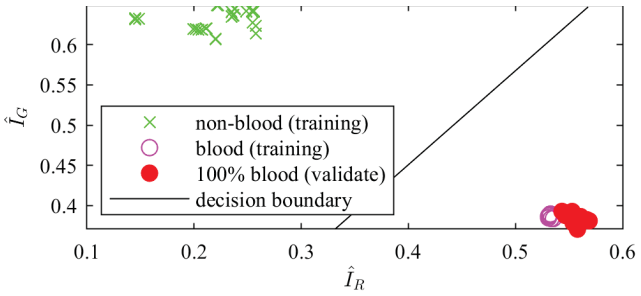

Fig. 11. The scatter plot using the normalised reflected green and red light intensity of the training and validation dataset are illustrated.

findings corroborate with that in [3], that blood demonstrates distinct absorbance in the at around $\lambda = 525$nm spectral region when compared to 0.9% saline solution. However, it is challenging to distinguish blood from similarly color haemoglobin-absent fluid, such as pomegranate juice and red food dye, as shown in Fig. 12. In this aspect, the proposed method of applying PCA and using the 1st PC, which is a linear combination of the normalised intensity of the reflected RGB light, for blood classification is superior. As shown in Fig. 10, the non-blood data which includes pomegranate juice and red dye forms a distinct cluster with tap water and saline.

IV. CONCLUSION

BWatch, a non-invasive continuous monitoring device for post-catheter insertion/extraction bleeding detection was presented. A simple threshold-based method based on the PCA using normalised RGB values were conceived. A binary SVM was trained on the 1st PC of blood and non-blood medium at the optimal intensity to derive the the single-value threshold for accurate detection. Significantly, the proposed approach is able to distinguish blood from similarly color haemoglobin-absent medium, preventing false positive detection. Also, BWatch achieved 100% detection rate across 10 clinical experiments with real blood. Future work will focus on assessing the performance of BWatch during in vivo clinical trial on actual CVC insertion/extraction site, and fine-tuning the design for better usability by medical staffs.

TABLE IV
DETECTION TIME AND BLOB AREA

Detection Time (s)		Blob Area (mm^2)	
Mean	Std.	Mean	Std.
4.88	0.85	1000	96

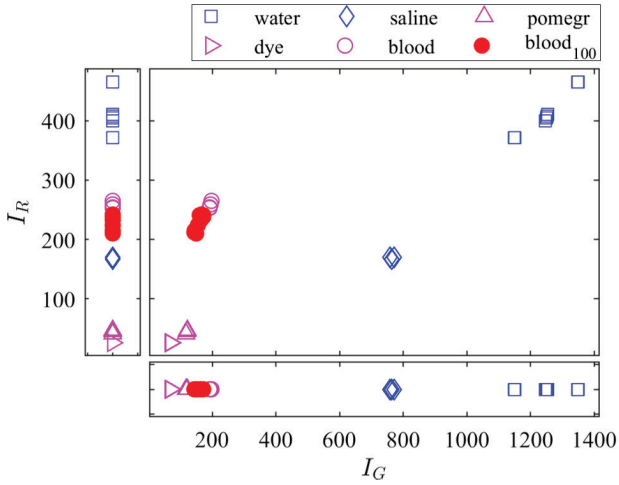

Fig. 12. The scatter plot using the unnormalised reflected green and red light intensity is illustrated.

REFERENCES

[1] P. Frykholm, A. Pikwer, F. Hammarskjöld, A. T. Larsson, S. Lindgren, R. Lindwall, K. Taxbro, F. Öberg, S. Acosta, and J. Åkeson, "Clinical guidelines on central venous catheterisation," *Acta Anaesthesiologica Scandinavica*, vol. 58, no. 5, pp. 508–524, 2014.

[2] R. Boersma and H. Schouten, "Clinical practices concerning central venous catheters in haematological patients," *European Journal of Oncology Nursing*, vol. 14, no. 3, pp. 200 – 204, 2010.

[3] J. P. F. Corts, T. H. Ching, C. Wu, C. Y. Chionh, S. Nanayakkara, and S. Foong, "Bward: An optical approach for reliable in-situ early blood leakage detection at catheter extraction points," in *2015 IEEE 7th International Conference on Cybernetics and Intelligent Systems (CIS) and IEEE Conference on Robotics, Automation and Mechatronics (RAM)*, July 2015, pp. 232–237.

[4] R. G. Haahr, S. B. Duun, M. H. Toft, B. Belhage, J. Larsen, K. Birkelund, and E. V. Thomsen, "An electronic patch for wearable health monitoring by reflectance pulse oximetry," *IEEE Transactions on Biomedical Circuits and Systems*, vol. 6, no. 1, pp. 45–53, Feb 2012.

[5] Y. Mendelson and B. D. Ochs, "Noninvasive pulse oximetry utilizing skin reflectance photoplethysmography," *IEEE Transactions on Biomedical Engineering*, vol. 35, no. 10, pp. 798–805, Oct 1988.

[6] J. M. Schmitt, "Simple photon diffusion analysis of the effects of multiple scattering on pulse oximetry," *IEEE Transactions on Biomedical Engineering*, vol. 38, no. 12, pp. 1194–1203, Dec 1991.

[7] Y. Khan, D. Han, A. Pierre, J. Ting, X. Wang, C. M. Lochner, G. Bovo, N. Yaacobi-Gross, C. Newsome, R. Wilson, and A. C. Arias, "A flexible organic reflectance oximeter array," *Proceedings of the National Academy of Sciences*, vol. 115, no. 47, pp. E11 015–E11 024, 2018. [Online]. Available: https://www.pnas.org/content/115/47/E11015

[8] K.-U. Jagemann, C. Fischbacher, K. Danzer, U. A. Mueller, and B. Mertes, "Application of near-infrared spectroscopy for non-invasive determination of blood/tissue glucose using neural networks," *Zeitschrift für Physikalische Chemie*, vol. 191, no. 2, pp. 179–190, 1995.

[9] S. Laha, S. Kaya, N. Dhinagar, Y. Kelestemur, and V. Puri, "A compact continuous non-invasive glucose monitoring system with phase-sensitive front end," in *2018 IEEE Biomedical Circuits and Systems Conference (BioCAS)*, Oct 2018, pp. 1–4.

[10] Avago Technologies, *Surface Mount LED Indicator*. ASMT-UxB5-Nxxxx Datasheet, May 2011.

[11] Texas Advanced Optoelectronic Solutions, *TCS3472 Color Light-to-Digital Converter with IR Filter*. TAOS135 Data Sheet, August 2012.

[12] I. Jolliffe, *Principal component analysis*. Springer, 2011.

[13] T. Hastie, R. Tibshirani, J. Friedman, and J. Franklin, "The elements of statistical learning: data mining, inference and prediction," *The Mathematical Intelligencer*, vol. 27, no. 2, pp. 83–85, 2005.